Progress In Electromagnetics Research B, Vol. 33, 339–358, 2011

PEER-TO-PEER LOCALIZATION IN URBAN AND INDOOR ENVIRONMENTS

S. W. Chen, S. Y. Tan*, and C. K. Seow

School of Electrical and Electronic Engineering, Nanyang Technological University, Singapore 639798, Singapore

Abstract—This paper presents a novel peer-to-peer or mobile-to-mobile localization scheme for general indoor and outdoor environments. In this scheme, two mobile nodes at arbitrary locations are able to locate each other without the need of Line-of-Sight (LOS) path between the two mobile device, and without the need for any reference devices such as GPS or land base beacons. Existing peer-to-peer localization techniques make use of Time of Arrival (TOA) and Angle of Arrival (AOA) of LOS and single bounce scattering paths to derive line of possible mobile device positions (LPMDs). The intersections of LPMDs are then used to estimate the unknown mobile device position — referred to as the Line Segment Intersection. However, in a heavy multipath environment with many multiple-bounce scattering paths, existing techniques require weighting factors and threshold values which are specifically chosen for that particular environment in order to select the LPMDs that correspond to LOS and single-bounce scattering paths for localization. Large localization error will occur if multiple-bounce scattering paths' LPMDs are mistakenly used for intersections. In addition, existing techniques also do not work well in a multipath environment with high level of TOA and AOA noises especially when the angles between LPMDs are small. The accuracy of the Line Segment Intersection also deteriorates as the distance traveled by multipath signals become comparable to each other. This renders the weighting and threshold values ineffective. This paper presents a novel Gaussian weighting process to remove the abovementioned limitations. The Gaussian weighting process also dramatically improves the accuracy of the localization. Experimental coupled with simulation results show that our proposed localization scheme outperforms existing Peer-to-peer localization technique by a significant margin of up to 83% and 54%

Received 7 July 2011, Accepted 8 August 2011, Scheduled 14 August 2011

* Corresponding author: Soon Yim Tan (esytan@ntu.edu.sg).

in indoor and urban environments respectively especially under severe multipath propagation conditions and high level of TOA and AOA noises.

1. INTRODUCTION

There is a great need for accurate and robust techniques for peer-to-peer or mobile-to-mobile localization in wireless and sensor networks [1–4]. The most important applications include localization services for mobile ad hoc networks (MANET), vehicular ad hoc network (VANET), and emergency 911 (E-911) caller to Public Safety Answering Points (PSAPs) [2]. However, there are many challenges, including channel fading, low signal to noise ratio, multiuser interference and multipath. In addition, there is a need for ubiquitous localization even in indoor environments where multipath tends to be more dominant [5]. Many indoor wireless localization methods using the UWB radio channel, WLAN-based and channel impulse response based techniques have been proposed [6–10].

Under conventional localization scheme, at least 3 reference devices (RDs) in Line of Sight (LOS) are needed to locate the mobile device (MD) in 2-D environment. The Euclidian distance between RD and MD is measured from the received signal. The geometrical relation between them is then used to obtain the estimated MD position [11].

The data that are used for localization can be the measured Time Difference of Arrival (TDOA) [12, 13], Time of Arrival (TOA) [14, 15], the angle of arrival (AOA) [16] or the Received Signal Strength (RSS) [17]. There is also a hybrid scheme that uses a combination of TOA, AOA and RSS [18–20].

Conventional LOS schemes suffer when there are not enough RDs in LOS with the MD or when multipath is very dominant [21]. Many multipath mitigation techniques [22–29] have been proposed to mitigate the problem of Non-Line-of-Sight (NLOS) propagation. These techniques are still unable to overcome the problem of insufficient number of RDs, which are in LOS with the MD. It has been proven that with the knowledge of NLOS information [29–31], localization performance will be greatly enhanced. Furthermore, NLOS localization schemes [32–34] not only do not leverage any RD that is in LOS with MD for localization but also enable accurate Peer-to-peer localization capability. Peer-to-peer localization has been a prevalent research topic especially in wireless cooperative network [35, 36]. In the context of Peer-to-peer Localization, only the neighbouring peer (only one RD) is needed to be in LOS with the MD. In simplistic context, it is a mobile-to-mobile or one RD to MD

localization. However, in multipath environment, the neighbouring peer may be in NLOS too. In [32, 33], NLOS information, like those of one bounce scattering, is not discarded but used to complement LOS information (if any) in determining MD position. Briefly, TOA and AOA measured with each one bounce scattering paths can be manipulated to form a line on which the unknown mobile device is most likely contained — referred to as Line of Possible Mobile Device location (LPMD). In [32], each LPMD is assigned appropriately with a weighting factor based on propagation distance between RD and MD, and a selection process is proposed to choose LPMDs with weighting factors above certain thresholds. The main drawback of this approach is that the weighting factor for each LPMD and the threshold value are adjusted accordingly for different environments. Furthermore, the scheme used in [32] do not work well in environments when multipath becomes too dominant or the distances travelled by multiple-bounce signal paths become comparable with those of one-bounce signal, causing weighting factors of multiple-bounce path LPMDs to be comparable with those from one-bounce.

In this paper, we formulate a novel Peer-to-peer (mobile-to-mobile/one RD to mobile) localization scheme to improve the robustness of the method used in [32]. More importantly, our proposed scheme does not require specifically adjusted weighting factors/threshold value to select the LPMDs for localization. The robustness and accuracy of the technique are also greatly enhanced by our proposed Gaussian weighting process that does not require any threshold value to select the LPMD for localization. The rationale of this Gaussian weighting process is that since each measurement metric contains noise, the intersection point between a pair of LPMDs will also contain noise. The amount of noise variance of each intersection point can be determined analytically and it depends on many factors such as distance travelled and relative alignments of LPMD pairs that form the intersection point. The proposed scheme will then construct a Gaussian weighting function of each intersection point using the calculated variance, and assign weights to intersection points based on how close these points are to the intersection point of interest by using Gaussian weighting function. Intersection points that have smaller variances will assign less weight to their neighbors and more weight to themselves and vice versa. This process removes the need for specifically chosen weighting factors and threshold values. Our proposed localization technique has also shown to be robust and outperformed existing Peer-to-peer localization technique by a significant margin for various indoor and outdoor environments.

2. THEORY AND FORMULATION

2.1. Concept of Line of Possible Mobile Device Location (LPMD) and Line Segment Intersection

The concept of Line of Possible Mobile Device (LPMD) in a 2-D environment has been introduced in Seow and Tan [32]. It uses LOS and one-bounce signal paths to find possibilities of MD's position. In Seow and Tan methodology, each propagation path associated between each RD and MD has the measured TOAs and azimuth AOAs at both RD and MD (a pair of TOA and AOA at each side for every path). These four TOA and azimuth AOA parameters for each path at the RD and MD pair can be extracted and measured using the super resolution techniques such as Parametric Subspace-Based Estimation (PSBE) and the Deterministic Parameter Estimation (DPE) in the light of MUltiple SIgnal Classification (MUSIC), Space Alternating Generalized EM (SAGE) respectively [37, 38]. In Seow and Tan experiment, SAGE algorithm is adopted. The measured TOAs and AOAs for each associated path between a RD and MD pair is then used to construct the LPMD that depicts the likely MD locations. These LPMDs are constructed on the context that their associated paths undergo LOS or one bounce reflection or diffraction. As shown in Fig. 1 [32] for Seow and Tan methodology, there are 3 RDs and 1 MD in the actual multipath environment in Nanyang Technological University. Two dominant paths are extracted using SAGE algorithm for each RD and MD pair, which translate to 6 LPMD lines.

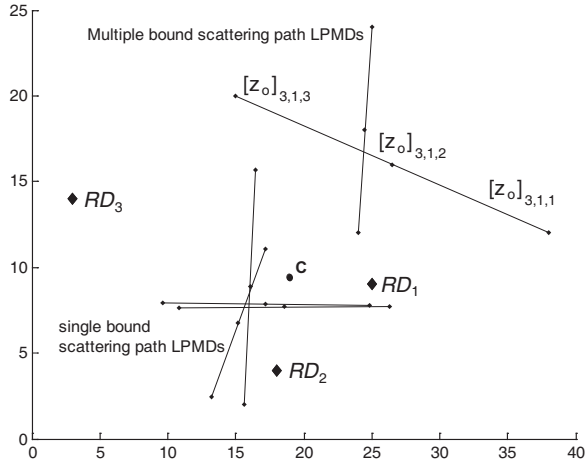

Figure 1. LPMDs cluster map in Nanyang Technological University at school of EEE faulty block with MD location at coordinate (16, 8) [32].

Upon construction of LPMDs, Seow and Tan methodology in [32] proposes the calculation of the centroid **C** for these LPMDs. As shown in Fig. 1, which is the typical multipath environment, LOS and the one-bounce signal paths' LPMDs will cluster together and multiple bounce signal paths' LPMDs will be the outliers. Therefore, through the calculation of the centroid of all LPMDs, we will be able to isolate the multiple bounce signal paths' LPMDs. To enhance the identification of the LOS and one bounce signal paths' LPMDs through the calculation of centroid C, a weighting factor for each LPMD has been included in the centroid **C** computation. The weightage factor for LOS and the one-bounce signal paths will be much higher as compared to multiple bounce signal paths. This is because the propagation distance between a RD and MD is always the shortest for LOS path as compared to NLOS multi bounce paths.

Once the centroid has been computed, the selection of LPMDs is done through the nearest distance to the centroid. As such, the multiple bounce paths' LPMDs can be accurately isolated. The final step will be the line segment intersection of the LOS and one-bounce signal paths' LPMDs in order to give rise to the correct MD location. The above formed the basis of Seow and Tan localization scheme.

2.2. Proposed Concept of Proximate Points

In a dense multipath environment such as an indoor scenario, localization is difficult due to abundance of low height scatterers [39]. Seow and Tan algorithm in [32] may not work well if the multiple bounce signal paths are abundant, as the centroid will be pivoted towards the multiple bounce signal paths' LPMDs rather than LOS and one bounce signal paths' LPMDs. However the ceiling one-bounce reflected paths, which are usually dominant in such environment, could be used to enhance the robustness of LPMD identification and hence the localization accuracy. However, if the problem is to be extended to 3-D, the LPMDs, in general, will not intersect with each other. This is where the concept of proximate point comes into picture. Proximate points are points on each LPMD in a LPMD pair in which the distance between those 2 points is minimized. This section will describe the formulation of LPMD in full 3-D, so that multipath propagation including ceiling and general reflections can be used for localization. Fig. 2 depicts proximate points $P_{a,1}$ and $P_{a,2}$ of a LPMD-pair. In subsequent sections, those two paired proximate points are combined together by taking their average to form P_a. Hence there is only one proximate point per LPMD pair. As the $P_{a,1}$ and $P_{a,2}$ are the shortest distance projection of the difference vector of the LPMP

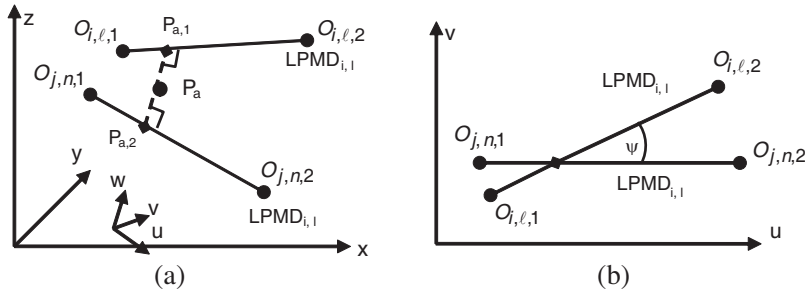

Figure 2. (a) A pair of LPMD and its corresponding proximate points and (b) its projection onto UV-plane.

pair $(\vec{P}_{a,2} - \vec{P}_{a,1})$ on each respective LPMD, a new coordinate that is u, v and w axes will be introduced to replace the conventional x, y, z coordinates to simplify the formulation. In this new coordinate system, w-axis is parallel to the vector between $P_{a,1}$ and $P_{a,2}$ in Fig. 2. U-axis is defined as the axis that is in the direction of one of the LPMDs in the pair, and v-axis as the orthogonal axis. The following notations are defined with known RDs' locations.

- $dr'_{i,\ell}$: Distance measured by RD_i for lth path from MD to RD_i.
- $dm'_{i,\ell}$: Distance measured by MD for lth path from RD_i to MD.
- $\phi r'_{i,\ell}$: Azimuth AoA of lth path from MD as measured by RD_i.
- $\phi m'_{i,\ell}$: Azimuth AoA of lth path from RD_i as measured by MD.
- $\theta r'_{i,\ell}$: Zenith AoA of lth path from MD as measured by RD_i.
- $\theta m'_{i,\ell}$: Zenith AoA of lth path from RD_i as measured by MD.
- $\hat{MD} = (\hat{X}_m, \hat{Y}_m, \hat{Z}_m)$: Estimated MD's position.

where $i, j = 1, 2 \ldots N$ where N is the total number of RD in the environment. $l, n = 1, 2 \ldots L$ where L is the total number of paths that can be traced from a particular RD.

The prime in the above variables denotes measurement metrics with noise component inside them. For example: $\phi r'_{i,l} = \phi r_{i,l} + n(0, \sigma_\phi)$ where $\phi r_{i,l}$ is the true azimuth AOA at RD_i and the noise is assumed to be Gaussian with zero mean and standard deviation of σ_ϕ. Similarly, $dm'_{i,l} = dm_{i,l} + n(0, \sigma_d)$. Zenith angle is angle formed between vertical axis ($+z$ axis) and the signal vector whereby azimuth angle is the angle formed in the horizontal plane (XY-plane) between $+x$-axis and the signal vector as projected to XY-plane. The equations for 2-D LPMD

have been derived previously in [32]. Extending it to 3-D, we can obtain the following equations:

$$\begin{aligned} Xo_{i,\ell,k} &= Xi + d'_{i,\ell} \times \cos(\alpha) \times \sin(\beta) \\ Yo_{i,\ell,k} &= Yi + d'_{i,\ell} \times \sin(\alpha) \times \sin(\beta) \\ Zo_{i,\ell,k} &= Zi + d'_{i,\ell} \times \cos(\beta) \end{aligned} \tag{1}$$

where coordinates of $O_{i,\ell,k}$ are ($Xo_{i,\ell,k}$, $Yo_{i,\ell,k}$, $Zo_{i,\ell,k}$), and k is 1 or 2 for $\alpha = \phi r'_{i,l}$, $\beta = \theta r'_{i,l}$, $d'_{i,l} = dr'_{i,l}$ or $\alpha = \phi m'_{i,l}$, $\beta = \theta m'_{i,l}$, $d'_{i,l} = dm'_{i,l}$ respectively. Coordinate (X_i, Y_i, Z_i) are the RD_i position.

Consider the two LPMDs as shown in Fig. 2, and based on the relationship where $(\vec{P}_{a,2} - \vec{P}_{a,1}) \cdot e_{a,1} = 0$ and $(\vec{P}_{a,2} - \vec{P}_{a,1}) \cdot e_{a,2} = 0$, the proximate points of the LPMD pair can be calculated:

$$\vec{P}_{a,1} = \vec{r}_{a,1} + \lambda_0 \vec{e}_{a,1}, \quad \vec{P}_{a,1} = \vec{r}_{a,2} + \mu_0 \vec{e}_{a,2} \tag{2}$$

where $\vec{e}_{a,1}$, $\vec{e}_{a,2}$ are unit vectors in the direction of each LPMD, $\widehat{r}_{a,1}$, $\widehat{r}_{a,2}$ are points on each LPMD and $\vec{r}_{a,12} = \widehat{r}_{a,2} - \widehat{r}_{a,1}$ with $\mu_0 = -\frac{(\vec{r}_{a,12} \cdot \vec{e}_{a,1}) - (\vec{r}_{a,12} \cdot \vec{e}_{a,2})(\vec{e}_{a,1} \cdot \overleftarrow{e}_{a,2})}{1 - (\vec{e}_{a,1} \cdot \vec{e}_{a,2})}$, $\lambda_0 = \frac{(\vec{r}_{a,12} \cdot \vec{e}_{a,1}) - (\vec{r}_{a,12} \cdot \vec{e}_{a,2})(\vec{e}_{a,1} \cdot \overleftarrow{e}_{a,2})}{1 - (\vec{e}_{a,1} \cdot \vec{e}_{a,2})^2}$. Coordinate P_a is derived as the average of the $\widehat{P_{a,1}}$ and $\widehat{P_{a,2}}$.

2.3. Localization Scheme

2.3.1. Gaussian Weighting Process

To enhance accuracy, a weighting factor is assigned to each LPMD and its corresponding proximate points. The weighting factor of each LPMD is chosen to be inversely proportional to the square of the distance traveled of that particular LPMD. Each weighting factor is also normalized with respect to other weighting factors. It is formulated as follows:

$$W_{i,l} = \frac{\frac{1}{(d'_{i,l})^2}}{\sum_{i=1}^{N} \sum_{l=1}^{L} \left(\frac{1}{(d'_{i,l})^2} \right)} \tag{3}$$

After assigning weight to each LPMD, the next step is to find proximate points of all possible combinations of LPMD pairs (as discussed in Section 2.2) and calculate corresponding weighting factors. The weighting factor of each proximate point depends on the weighting factor of each LPMD in the LPMD pair and the angle between two LPMDs. In general, the smaller the angle between two LPMD pair, the greater the likelihood that the solution to proximate point's position

is ill conditioned. Hence we should assign less weight to LPMD pairs that have smaller angles between them.

$$Wp_a = \left(\frac{W_{j,n} \times W_{i,\ell}}{W_{j,n} + W_{i,\ell}}\right) \times \sin\Psi, \quad (i \neq j) \cup (\ell \neq n) \tag{4}$$

where $i, j = 1, 2 \ldots N$ where N is the total number of RD in the environment. $l, n = 1, 2 \ldots L$ where L is the total number of paths that can be traced from a particular RD. $a = 1, 2 \ldots A$ where A is the number of proximate points existing in the environment. Ψ : Angle between the LPMD pair in uv-plane (Fig. 2).

The next step is to calculate the Gaussian weighting. It is calculated by taking into account proximate point's individual weighting factor and weighting factors of its surrounding proximate points. The weighting factor of neighborhood proximate points is inversely proportional to their distances to the proximate point of interest. It is formulated as follows:

$$Wn_a = \sum_{b=1}^{K} \frac{Wp_b}{\sigma_{p_a}\sqrt{2\pi}} \times \exp\left(\frac{-\left\|\widehat{p}_b - \widehat{p}_a\right\|}{2\sigma_{p_a}^2}\right) \tag{5}$$

where σ_{pa} is the error standard deviation of the position of proximate point a. $\widehat{p}_b, Wp_b$ = Coordinate and weighting factor of proximate point b respectively.

The Gaussian weighting function takes the form of a Gaussian distribution function. Given the variance of a proximate point, the likelihood of that proximate point lying within a certain distance from the mean can be modeled and calculated by a Gaussian distribution function, with $\widehat{P}_a$ being assumed to be the mean of the Gaussian distribution. The MD position can be finally calculated as follows:

$$\hat{MD} = \frac{1}{K}\sum_{a=1}^{K}(\widehat{P}_a \times Wn_a) \tag{6}$$

where $\widehat{P}_a = (X_a, Y_a, Z_a)$: Coordinate of a-th proximate point. $\hat{MD} = \left(\hat{X}_m, \hat{Y}_m, \hat{Z}_m\right)$: Estimated coordinate of the mobile device. K: No. of proximate points in the environment.

The error standard deviation and variance of each proximate point will be formulated in next section.

2.3.2. Error Variance of Proximate Point

The error variance is useful for determining the reliability of each proximate point, and it will be used in (5) to determine the Gaussian

weighting. In order to simplify the calculation, throughout the variance calculation, it is assumed that the angle and distance measurement errors are normally distributed with zero mean and known standard deviation. The error standard deviation is assumed to be equal across all the RDs and MD. Before going into the detailed analysis we will first define:

$d_{i,\ell}^{uv}$: Distance traveled by lth path between MD and RD_i as projected on to UV-plane.

$\chi_{m_{j,n}}, \chi_{r_{j,n}}$: Elevation angle formed between AOA at MD and UV-plane and angle between AOA at RD_j and the UV-plane respectively.

$\xi_{m_{i,l}}, \xi_{r_{i,l}}$: Elevation angle formed between RD_i and one end of the $\text{LPMD}_{i,l}$ and between RD_i and the other end of the $\text{LPMD}_{i,l}$ respectively in the UV-plane.

$\tau_{i,\ell}$: Angle between the proximate point, one end of the $\text{LPMD}_{i,l}$ and RD_i in the UV-plane.

$\Delta\rho = \|\widehat{P}_a - \widehat{P}_a^{'}\| = \sqrt{\Delta\rho_u^2 + \Delta\rho_v^2 + \Delta\rho_w^2}$: Localization error of proximate point due to noise perturbation and $\widehat{P}_a^{'}$ is the proximate point perturbed by noise.

Perturbing one measurement variable at a time, and summing contributions from all measurement metrics obtain localization error variance of each proximate point. Total squared localization error can be obtained from squared summation of $\Delta\rho_u$, $\Delta\rho_v$, $\Delta\rho_w$ (localization error in U, V and W direction respectively) where

$$\begin{aligned}\Delta\rho_u = {} & \varepsilon_{\xi r_{i,\ell}^{uv}}\Delta\xi_{r_{i,\ell}}\cos\Psi + \varepsilon_{\xi m_{i,\ell}^{uv}}\Delta\xi_{m_{i,\ell}}\cos\Psi + \varepsilon_{d_{i,\ell}^{uv}}\Delta d_{i,\ell}\cos(\tau_{i,\ell})\cot\Psi \\ & + \varepsilon_{\chi r_{i,\ell}^{uv}}\Delta\chi_{r_{i,\ell}}\cos(\tau_{i,\ell})\cot\Psi + \varepsilon_{\chi m_{i,\ell}^{uv}}\Delta\chi_{m_{i,\ell}}\cos(\tau_{i,\ell})\cot\Psi \\ & + \varepsilon_{\xi r_{j,n}^{uv}}\Delta\xi_{r_{j,n}} + \varepsilon_{\xi m_{j,n}^{uv}}\Delta\xi_{m_{j,n}} + \varepsilon_{\chi r_{j,n}^{uv}}\Delta\chi_{r_{j,n}} \times (\cos(\tau_{j,n})\cot\Psi\cos\Psi \\ & + \cos(\tau_{j,n})\sin\Psi) + \varepsilon_{\chi m_{j,n}^{uv}}\Delta\chi_{m_{j,n}}(\cos(\tau_{j,n})\cot\Psi\cos\Psi + \cos(\tau_{j,n})\sin\Psi) \\ & + \varepsilon_{d_{j,n}^{uv}}\Delta d_{j,n}(\cos(\tau_{j,n})\cot\Psi\cos\Psi + \cos(\tau_{j,n})\sin\Psi) \end{aligned} \tag{7}$$

$$\begin{aligned}\Delta\rho_v = {} & \varepsilon_{\xi r_{i,\ell}^{uv}}\Delta\xi_{r_{i,\ell}}\sin\Psi + \varepsilon_{\xi m_{i,\ell}^{uv}}\Delta\xi_{m_{i,\ell}}\sin\Psi + \varepsilon_{d_{i,\ell}^{uv}}\Delta d_{i,l}\cos(\tau_{i,\ell}) \\ & + \varepsilon_{\chi r_{i,\ell}^{uv}}\Delta\chi_{r_{i,\ell}}\cos(\tau_{i,\ell}) + \varepsilon_{\chi m_{i,\ell}^{uv}}\Delta\chi_{m_{i,\ell}}\cos(\tau_{i,\ell}) \\ & + \varepsilon_{\chi r_{j,n}^{uv}}\Delta\xi_{r_{j,n}}(\cos(\tau_{j,n})\cot\Psi\sin\Psi + \cos(\tau_{j,n})\cos\Psi) \\ & + \varepsilon_{\chi m_{j,n}^{uv}}\Delta\xi_{m_{j,n}}(\cos(\tau_{j,n})\cot\Psi\sin\Psi + \cos(\tau_{j,n})\cos\Psi) \\ & + \varepsilon_{d_{j,n}^{uv}}\Delta d_{j,n}(\cos(\tau_{j,n})\cot\Psi\sin\Psi + \cos(\tau_{j,n})\cos\Psi) \end{aligned} \tag{8}$$

$$\begin{aligned}\Delta\rho_w = {} & \varepsilon_{\chi r_{i,\ell}^{w}}\Delta\chi_{r_{i,\ell}} + \varepsilon_{\chi m_{i,\ell}^{w}}\Delta\chi_{m_{i,\ell}} + \varepsilon_{d_{i,\ell}^{w}}\Delta d_{i,\ell} + \varepsilon_{\chi r_{j,n}^{w}}\Delta\chi_{r_{j,n}} \\ & + \varepsilon_{\chi m_{j,n}^{w}}\Delta\chi_{m_{j,n}} + \varepsilon_{d_{j,n}^{w}}\Delta d_{j,n} \end{aligned} \tag{9}$$

$\Delta\rho_u$, $\Delta\rho_v$, $\Delta\rho_w$ are derived by perturbing one variable at a time and

deducing the geometrical relations between the error of the variable and the distance between the initial and perturbed proximate point's position. It is assumed throughout the derivation that $\Delta\chi_r$, $\Delta\chi_m$, $\Delta\xi_r$ and $\Delta\xi_m$ are sufficiently small such that $\sin(\Delta\chi_r) \approx \Delta\chi_r$. Δ is defined as the small change in the parameter. Since all angle and distance measurement errors are statistically independent of each other, we have

$$\begin{aligned}
E(\Delta\rho_u^2) = &\left[\varepsilon_{\xi r_{i,\ell}^{uv}} \cos\Psi\right]^2 + \sigma_{\xi^2_{r_{i,\ell}}}\left[\varepsilon_{\xi m_{i,\ell}^{uv}} \cos\Psi\right]^2 + \sigma_{d^2_{i,\ell}}\left[\varepsilon_{d_{i,\ell}^{uv}} \cos(\tau_{i,\ell}) \cot\Psi\right]^2 \\
&+ \sigma_{\chi^2_{r_{i,\ell}}}\left[\varepsilon_{\chi r_{i,\ell}^{uv}} \cos(\tau_{i,\ell}) \cot\Psi\right]^2 + \sigma_{\chi^2_{m_{i,\ell}}}\left[\varepsilon_{\chi r_{i,\ell}^{uv}} \cos(\tau_{i,\ell}) \cot\Psi\right]^2 \\
&+ \sigma_{\xi^2_{m_{j,n}}}\left[\varepsilon_{\xi m_{j,n}^{uv}}\right]^2 + \sigma_{\xi^2_{r_{j,n}}}\left[\varepsilon_{\xi r_{j,n}^{uv}}\right]^2 \\
&+ \sigma_{d^2_{j,n}}\left[\varepsilon_{d_{j,n}^{uv}}\left(\cos(\tau_{j,n})\frac{\cos^2\Psi}{\sin\Psi} + \cos(\tau_{j,n})\sin\Psi\right)\right]^2 \\
&+ \sigma_{\chi^2_{r_{j,n}}}\left[\varepsilon_{\chi r_{j,n}^{uv}}\left(\cos(\tau_{j,n})\frac{\cos^2\Psi}{\sin\Psi} + \cos(\tau_{j,n})\sin\Psi\right)\right]^2 \\
&+ \sigma_{\chi^2_{m_{j,n}}}\left[\varepsilon_{\chi m_{j,n}^{uv}}\left(\cos(\tau_{j,n})\frac{\cos^2\Psi}{\sin\Psi} + \cos(\tau_{j,n})\sin\Psi\right)\right]^2 \qquad (10)
\end{aligned}$$

$$\begin{aligned}
E(\Delta\rho_v^2) = &\sigma_{\xi^2_{r_{i,\ell}}}\left[\varepsilon_{\xi r_{i,\ell}^{uv}} \sin\psi\right]^2 + \sigma_{\xi^2_{m_{i,\ell}}}\left[\varepsilon_{\xi m_{i,\ell}^{uv}} \sin\psi\right]^2 + \sigma_{d^2_{i,\ell}}\left[\varepsilon_{d_{i,\ell}^{uv}} \cos(\tau_{i,\ell})\right]^2 \\
&+ \sigma_{\chi^2_{r_{i,\ell}}}\left[\varepsilon_{\chi r_{i,\ell}^{uv}} \cos(\tau_{i,\ell})\right]^2 + \sigma_{\chi^2_{m_{i,\ell}}}\left[\varepsilon_{\chi m_{i,\ell}^{uv}} \cos(\tau_{i,\ell})\right]^2 \\
&+ \sigma_{d^2_{j,n}}\left[\varepsilon_{d_{j,n}^{uv}}(2\cos(\tau_{j,n})\cos\Psi)\right]^2 + \sigma_{\chi^2_{r_{j,n}}}\left[\varepsilon_{\chi r_{j,n}^{uv}}(2\cos(\tau_{j,n})\cos\Psi)\right]^2 \\
&+ \sigma_{\chi^2_{m_{j,n}}}\left[\varepsilon_{\chi m_{j,n}^{uv}}(2\cos(\tau_{j,n})\cos\Psi)\right]^2 \qquad (11)
\end{aligned}$$

$$\begin{aligned}
E(\Delta\rho_w^2) = &\sigma_{\chi^2_{r_{i,\ell}}}\left[\varepsilon_{\chi_{r_{i,\ell}^w}}\right]^2 + \sigma\chi^2_{m_{i,\ell}}\left[\varepsilon_{\chi_{m_{i,\ell}^w}}\right]^2 + \sigma_{d^2_{i,\ell}}\left[\varepsilon_{d_{i,\ell}^w}\right]^2 \\
&+ \sigma_{\chi^2_{r_{j,n}}}\left[\varepsilon_{\chi_{r_{j,n}^w}}\right]^2 + \sigma_{\chi^2_{m_{j,n}}}\left[\varepsilon_{\chi_{m_{j,n}^w}}\right]^2 + \sigma_{d^2_{j,n}}\left[\varepsilon_{d_{j,n}^w}\right]^2 \qquad (12)
\end{aligned}$$

Finally we can find the total distance error variance of each proximate point by:

$$\Delta p^2 = \Delta p_u^2 + \Delta p_v^2 + \Delta p_w^2, \quad E(\Delta p^2) = E(\Delta p_u^2) + E(\Delta p_v^2) + E(\Delta p_w^2) = \sigma_{p_a}^2 \qquad (13)$$

3. RESULTS AND DISCUSSION

To test the applicability and accuracy of our proposed peer-to-peer localization scheme, we compare our results with those presented in [32]

with two different indoor and outdoor environments [39, 43] as shown in Figs. 3 and 4. In these figures, RD denotes the reference mobile node, while the node to be localized with respect to RD is denoted as MD. For the indoor environment as shown in Fig. 3, the height between ceiling and floor is 2.6 m and the heights of all scatterers are 2 m. For the outdoor environment as shown in Fig. 4, all buildings are assumed to be much higher than RD and MD which are assumed to be at the height of 1m above ground. The authors in [32] presented the results of their proposed technique by selecting two best two LPMDs or one-bound scattering paths based on the following procedures: (1) each LPMD is assigned a weighting factor based on the propagation path length, (2) only LPMDs or paths that have weighting factors above certain threshold value are included in the calculation. The optimum threshold value in [32] is found to be 0.1. In our proposed scheme, two LPMDs are required to obtained one proximate point. In order to give a fair comparison, we will use one proximate point with the highest Gaussian weighting factor as formulated in (5) to estimate the MD position. Channel measurement on real environments [39, 43] were taken and the measured data metrics were verified according to the traditional ray tracing methodology [40–42] to obtain the data metrics of TOA and AOA for the two environments. The delay profile measurements were taken using a network analyzer. Fig. 3 traces the actual rays that run between the RD and MD. This is based on the correlation between the measured data metrics and the ray tracing methodology. For a rigorous comparison with [32], the noise free TOA and AOA of each signal path between RD and MD are subject to random TOA and AOA Gaussian noise with zero mean and a given variance. The root mean square (RMS) error σ_{rms} that is related to the true MD location is calculated as $\|MD - \hat{MD}\|$ where $\hat{MD}$ denote the estimated MD position. Each set of σ_{rms} is computed based on 10,000 independent simulation runs using MatLab.

RD is positioned at $(5, 2, 1)$ and two different MDs are at positioned $(13, 4, 1)$ and $(16, 8, 1)$ as shown in Figs. 3(a) and 3(b) respectively. In Fig. 3(a), RD is in LOS with MD and the signal paths that will be used for localization include the LOS, ceiling and floor reflected paths (solid lines) and three one-bounce wall reflection paths (dash-lines). Higher order scattering paths that must be mitigated include twelve two-bounce reflected paths (doted-line) and twenty-four three-bounce reflected paths (shown as doted-line). In Fig. 3(b), there is no direct LOS path between MD and RD. The shortest dominant propagation path is the ceiling reflected path, as shown as solid line. The ceiling reflected path and the two one-bounce wall reflected paths could be exploited to perform localization. Higher order scattering

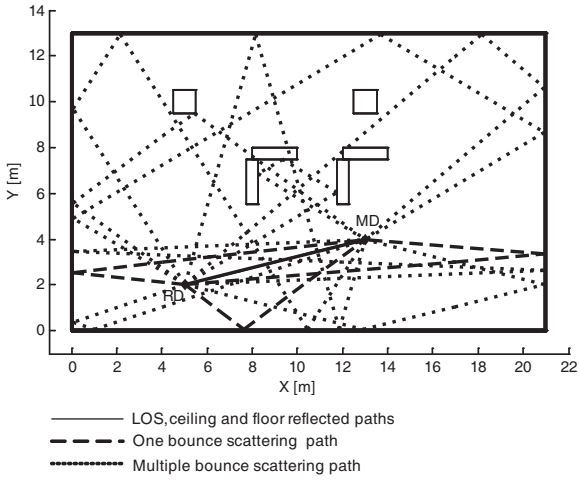

(a)

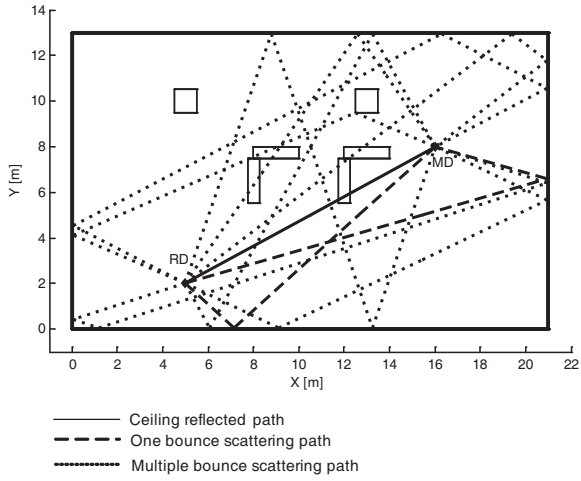

(b)

Figure 3. Indoor Environment (a) RD is in LOS with the MD (b) RD is in NLOS with the MD.

paths that may cause localization error include ten two-bounce and twenty-five three-bounce reflection paths.

Figure 5 depicts the location accuracy of our proposed Peer-to-peer localization scheme as compared with [32] via their cumulative probability distribution (CDF). The AOA standard deviations for both RD and MD (σ_θ and σ_ϕ) are chosen to be 4 degrees (and 8 degrees) while the distance standard deviations σ_d for both RD and

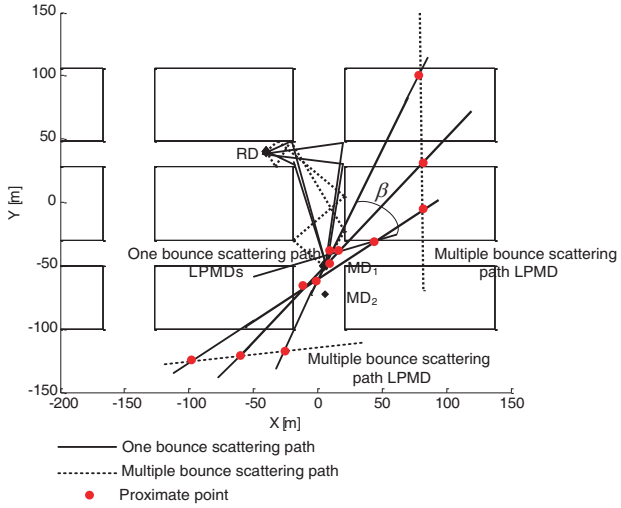

Figure 4. Outdoor environment showing scatterplot of the path's LPMD at MD_1.

Table 1. Propagation Distance and weighting factor for one bounce and multiple bounce scattering paths.

Number of reflection	Propagation Distance	Weighting factor of LPMD
One bounce scattering path	12.9 m	0.046
	14.8 m	0.040
	21.7 m	0.027
Two bounce scattering path	14.9 m	0.040
	15.1 m	0.039
	23.1 m	0.025
	33.6 m	0.018
Three bounce scattering path	15.7 m	0.038
	20 m	0.029
	22.7 m	0.026
	25.7 m	0.023
	55.1 m	0.011

MD are chosen to be 2 m (and 4 m) — referred to as Condition 1 and 2 respectively. In Fig. 5, ωth is the LPMD weighting threshold value used in [32] to choose the two best LPMDs for localization. In our simulation, we have simulated ωth from 0 to 0.1 and have chosen the optimum threshold value for comparisons. It is observed in Fig. 5 that our proposed scheme outperforms the existing Seow and Tan's technique by a significant margin. For example in LOS scenario (Fig. 5(a)) under condition 1: $\sigma_d = 2$ m, $\sigma_\theta = \sigma_\phi = 4^\circ$, our proposed Gaussian weighted schemes achieved an accuracy of 1.7 m for 90% of the time as compared to 2.4 m of Seow and Tan's in [32]. This represents an improvement of about 29%. The margin of improvement increased to 42% as the TOA and AOA noise increases to Condition 2: $\sigma_d = 4$ m, $\sigma_\theta = \sigma_\phi = 8^\circ$. In Fig. 5(b), MD is in NLOS with RD with very severe multipath propagation i.e., the distances traveled by many multiple-bounce paths are comparable or shorter than the one-bounce scattering paths making the weighting factors and threshold value in [32] ineffective. Table 1 shows the true propagation distance of single and multiple-bounce paths and their corresponding weighting factors for MD shown in Fig. 3(b). In this case, many multi-bounce paths have higher weighting compared with the single-bounce paths. Too high a threshold value may result in less than 2 paths that are required for localization. For example, only the ceiling reflected path would be chosen if ωth is more than 0.04. On the other hand, too low a threshold value will not be able to exclude the multiple-bounce paths. These multiple-bounce paths, if mistakenly used, will result in considerable errors. For example, under condition 1, our proposed Gaussian weighted scheme has achieved an accuracy of 1.6 m for 90% of the time as compared to 6.9 m (ωth = 0.03) and 9.2 m (ωth = 0.02) of Seow and Tan's in [32]. This represents a significant improvement of about 77% and 83% respectively as shown in Fig. 5(b).

To test the applicability and accuracy of our proposed scheme in a larger urban outdoor environment, Manhattan urban street-grid environment [43] are used with RD positioned at 40 meters from the cross junction and two different MD positions, MD_1 and MD_2 at 50 and 80 meters from the cross junction respectively. This is shown in Fig. 4. This simulated the MD following a path from MD_1 to MD_2 of 30 m distance difference. In this scenario, RD is in NLOS with MD_1 and MD_2 and there are only 4 corner diffracted paths that can be used for localization (solid lines in Fig. 4). In this case, there are two three-bounce building-reflected paths (dotted line) that should be excluded to avoid localization errors. Fig. 4 also shows the LPMDs for all the major propagation paths at MD_1. Similar to the indoor environment in Fig. 3, the AOA standard deviations at both RD and MD are chosen to

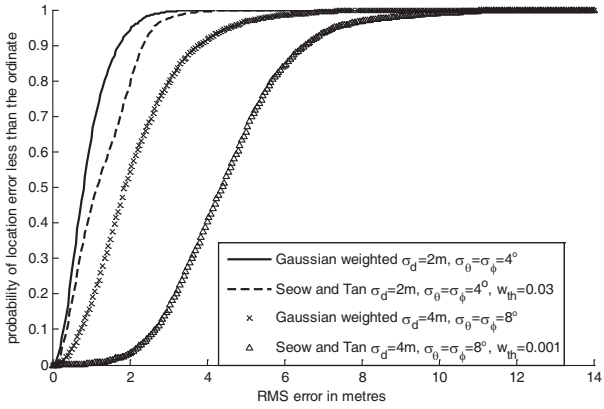

(a)

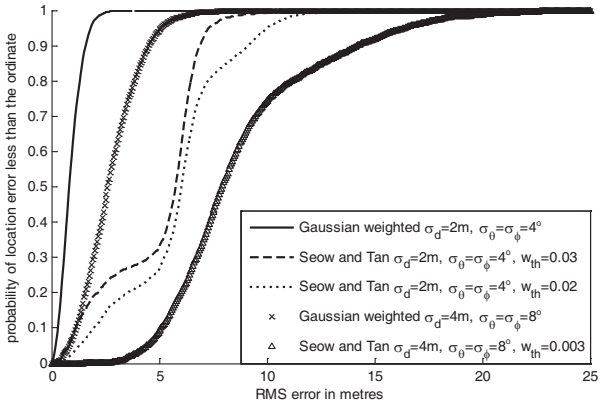

(b)

Figure 5. (a) Comparison of CDF performance for MD located at $(13, 4, 1)$ — RD is in LOS with MD. (b) Comparison of CDF performance for MD located at $(16, 8, 1)$ — RD is in NLOS with MD.

be 4 degrees and 8 degrees while the corresponding distance standard deviations σ_d for both RD and MD are chosen to be 2 m and 4 m.

It is observed from the simulation results, as illustrated in Fig. 6, our proposed scheme outperforms the existing Line Segment Intersection technique by a significant margin especially when MD is moved away from the cross junction. For example, for MD_1 which is positioned at 50 meters from the cross junction, and using $\sigma_d = 2$ m, $\sigma_\theta = \sigma_\phi = 4^\circ$, Fig. 6 shows that our proposed scheme achieves an accuracy of 22 m for 90% of the time as compared 31.5 m (ωth = 0.16) of Seow and Tan's Line Segment Intersection in [32]. An improvement of about 30% is shown in Fig. 6. This margin increases to 53% for MD_2,

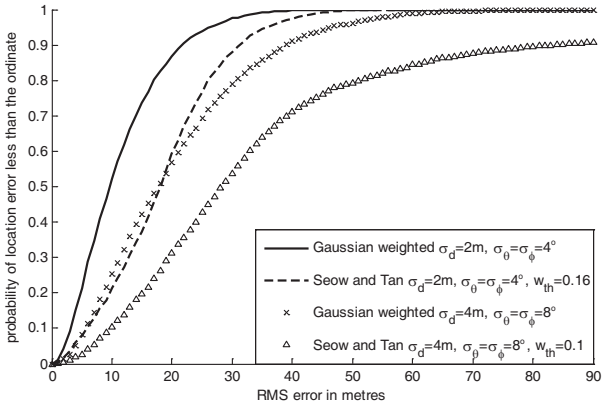

Figure 6. Comparison of CDF performance for MD located at $(5, -50, 1)$.

which is located further away of about 80 meters from the junction. The accuracy of the Line Segment Intersection deteriorates due to the fact that as the distance becomes larger, the angles between LPMDs, β, will become smaller. The Line Segment Intersection will not work well under this condition especially under high TOA and AOA noise. In our proposed Gaussian weighting method, the weight of each proximate point is assigned based on the proximity of other proximate points. The smaller the distance between each neighborhood proximate point and proximate point of interest, the larger the weight will be assigned. As shown in Fig. 4, the proximate points due to the 4 corner-diffracted paths are close to each other as compared with those involving three-bounce building reflected paths. As the noise increases to $\sigma_d = 4\,\text{m}$, $\sigma_\theta = \sigma_\phi = 8°$, our proposed scheme has an accuracy of about 39 m as compared to 85 m of Seow and Tan's Line Segment Intersection in [32] for a mobile device located at MD_1 The improvement is about 54%.

Overall, our proposed scheme has outperformed the Line Segment Intersection technique in [32] in all cases. The margin of improvement increases as the distance between RD and MD becomes larger (or the angles between LPMDs become smaller) and our proposed scheme is robust under high TOA and AOA noise and severe multipath conditions.

4. CONCLUSION

A novel approach of peer-to-peer NLOS localization scheme using proximate points and Gaussian weighting process has been proposed with the main advantage of being able to work robustly in dense

multiple environment. It has been demonstrated experimentally and coupled with simulations in two typical indoor and outdoor environments that our proposed 3D NLOS localization scheme outperforms the existing NLOS localization scheme in all cases in relation to various degree of TOA and AOA measurement noise. Location error standard deviation σ_{rms} of less than 1.6 m and 22 m for 90% of time for the indoor and outdoor environment respectively have been obtained.

REFERENCES

1. Patwari, N., J. N. Ash, S. Kyperountas, A. O. Hero III, R. L. Moses, and N. S. Correal, "Locating the nodes: Cooperative localization in wireless networks," *IEEE Signal Processing Mag.*, Vol. 22, 54–69, Jul. 2005.
2. Sayed, A. H., A. Tarighat, and N. Khajehnouri, "Network-based wireless location: Challenges faced in developing techniques for accurate wireless location information," *IEEE Signal Processing Mag.*, Vol. 22, 24–40, Jul. 2005.
3. Wang, Z. H. and S. A. Zekavat, "A novel semi-distributed cooperative localization technique for MANET: Achieving high performance," *Proc. IEEE Wireless Communications Networking Conf.*, 2414–2419, 2008.
4. Boukerche, A., H. A. B. F. Oliveira, E. F. Nakamura, and A. A. F. Loureiro, "Vehicular Ad Hoc networks: A new challenge for localization-based systems," *Computer Communications*, Vol. 31, No. 12, 2838–2849, Jul. 2008.
5. Tan, S. Y. and H. S. Tan, "Modelling and measurements of channel impulse response for an indoor wireless communication system," *Proc. IEE Microwaves, Antennas and Propagation, Part H*, Vol. 142, No. 5, 405–410, Oct. 1995.
6. Jin, Y., W. S. Soh, and W. C. Wong, "Indoor localization with channel impulse response based fingerprint and nonparametric regression," *IEEE Trans. Wireless Commun.*, Vol. 9, 1120–1127, 2010.
7. Tayebi, A., A, J. Gomez, F. S. De Adana, and O. Gutierrez, "Ray-tracing application to mobile localization in multipath indoor environments," *Proc. ICEAA 2009*, 412–415, Torino, Italy, Sep. 2009.
8. Deasy, T. P. and W. G. Scanlon, "Stepwise algorithms for improving the accuracy of both deterministic and probabilistic

methods in WLAN-based indoor user Localization," *Int. J. Wireless Information Networks*, Vol. 11, Oct. 2004.

9. Lee, J. Y. and R. A. Scholtz, "Ranging in a dense multipath environment using an UWB radio link," *IEEE J. Select. Areas Commun.*, Vol. 20, 1677–1683, Dec. 2002.
10. Tai, C. S., S. Y. Tan, and C. K. Seow, "A robust non-line-of-sight localization system in indoor environment," *IET Electronics Letters*, Vol. 46, No. 8, 593–595, 2010.
11. Bao-Yen Tsui, J., *Fundamentals of Global Positioning System Receivers: A Software Approach*, John Wiley & Sons, 2005.
12. Liew, S. C., K. G. Tan, and T. S. Lim, "Investigation of direct A-GPS positioning for hybrid E-OTD/GNSS," *Journal of Electromagnetic Waves and Applications*, Vol. 20, No. 1, 79–87, 2006.
13. Chan, Y. T. and K. C. Ho, "A simple and efficient estimator for hyperbolic location," *IEEE Trans. Signal Processing*, Vol. 42, 1905–1915, Aug. 1994.
14. Lui, K. W. K. and H. C. So, "Range-based source localisation with pure reflector in presence of multipath propagation," *IEE Electronics Letters*, Vol. 46, No. 13, 957–958, 2010.
15. Chueng, K. W., H. C. So, W.-K. Ma, and Y. T. Chan, "Least square algorithms for time-of-arrival based mobile location," *IEEE Trans. Signal Processing*, Vol. 52, 1121–1128, Apr. 2004.
16. Alba, P. Z., V. Josep, and D. H. Brooks, "Closed form solution for positioning based on angle of arrival measurements," *Proc. IEEE Int. Symp. Personal Indoor Mobile Radio Commun. Conf.*, Vol. 14, 1522–1526, 2002.
17. Patwari, N., A. O. Hero III, M. Perkins, N. S. Correal, and R. J. O. Dea, "Relative location estimation in wireless sensor networks," *IEEE Trans. Signal Processing*, Vol. 51, 2137–2148, Aug. 2003.
18. Zhang, V. Y. and A. K.-S. Wong, "Combined AOA and TOA NLOS localization with nonlinear programming in severe multipath environments," *Proc. IEEE Trans. Wireless Commun. Networking Conf. (WCNC'09),* 1–6, Apr. 2009.
19. Tayebi, A., J. Gomez, F. Saez de Adana, and O. Gutierrez, "The application of ray-tracing to mobile localization using the direction of arrival and received signal strength in multipath indoor environments," *Progress In Electromagnetic Research*, Vol. 91, 1–15, 2009.

20. Xie, Y., Y. wang, P. Zhu, and X. You, "Grid-search-based hybrid TOA/AOA location techniques for NLOS environments," *IEEE Communications Letters*, Vol. 13, No. 4, 254–256, 2009.
21. Jiang, L. and S. Y. Tan, "Geometrical-based statistical channel model for outdoor and indoor propagation environments," *IEEE Trans. Vehicular Technology*, Vol. 56, No. 6, 3587–3593, Nov. 2007.
22. Wang, X., Z. X. Wang, and B. O. Dea, "A TOA-based location algorithm reducing the errors due to Non-Line-of-Sight (NLOS) propagation," *IEEE Trans. Vehicular Technology*, Vol. 52, 112–116, Jan. 2003.
23. Khajehnouri, N. and A. H. Sayed, "A non-line-of-sight equalization scheme for wireless cellular location," *Proc. ICASSP 2003*, Vol. 6, 549–552, Apr. 2003.
24. Chen, P. C., "A non-line-of-sight error mitigation algorithm in location estimation," *Proc. IEEE Wireless Communications Networking Conf.*, Vol. 1, 316–320, 1999.
25. Cong, L. and W. H. Zhuang, "Nonline-of-sight error mitigation in mobile location," *IEEE Trans. Wireless Commun.*, Vol. 4, 560–572, Mar. 2005.
26. Xiong, L., "A selective model to suppress NLOS signals in angle of arrival (AOA) location estimation," *Proc. IEEE Int. Symp. Personal, Indoor and Mobile Radio Commun.*, Vol. 1, 461–465, 1998.
27. Chan, Y. T., W. Y. Tsui, H. C. So, and P. C. Ching, "Time-of-arrival based localization under NLOS conditions," *IEEE Trans. Vehicular Technology*, Vol. 55, 17–24, Jan. 2006.
28. Borras, J., P. Hatrack, and N. B. Mandayam, "Decision theoretic framework for NLOS identification," *Proc. IEEE Veh. Tech. Conf.*, Vol. 2, 1583–1587, 1998.
29. Bahillo Martinez, A., S. Mazuelas Franco, J. Prieto Tejedor, R. M. Lorenzo Toledo, P. Fernandez Reguero, and E. J. Abril, "Indoor location based on IEEE 802.11 round-trip time measurements with two-step NLOS mitigation," *Progress In Electromagnetic Research B*, Vol. 15, 285–306, 2009.
30. Qi, Y. H., H. Kobayashi, and H. Suda, "Analysis of wireless geolocation in a non-line-of-sight environment," *IEEE Trans. Wireless Commun.*, Vol. 5, 672–681, Mar. 2006.
31. Shen, Y. and M. Z. Win, "Fundamental limits of wideband localization-Part 1: A general framework," *IEEE Trans. Information Theory*, Vol. 56, 4956–4980, Oct. 2010.
32. Seow, C. K. and S. Y. Tan, "Non line of sight localization in

multipath environment," *IEEE Trans. Mobile Computing*, Vol. 7, No. 5, 647–660, May 2008.

33. Seow, C. K. and S. Y. Tan, "Localization of omni-directional mobile device in multipath environments," *Progress In Electromagnetic Research*, Vol. 85, 323–348, 2008.
34. Miao, H. L., K. Yu, and M. J. Juntti, "Positioning for NLOS propagation: "Algorithm derivations and cramer-rao bounds," *Proc. ICASSP 2006*, Vol. 4, 1045–1048, Jun. 2006.
35. Sottile, F., M. A. Spirito, M. A. Cacere, and J. Samson, "Distributed-weighted multidimensional scaling for hybrid peer-to-peer localization," *Proc. IEEE Ubiquitous Positioning Indoor Navigation and Location Based Service Conf.*, Dec. 2010.
36. Ekambaram, V. N. and K. Ramchandran, "Distributed high accuracy peer-to-peer localization in mobile multipath environments," *Proc. IEEE GlobeCom*, Dec. 2010.
37. Stocia, P. and A. Nehorai, "MUSIC, maximum likelihood and Cramer-Rao Bound," *IEEE Trans ACSSP*, Vol. 37, 720–741, May 1989.
38. Fluery, B. H., M. Tschudin, R. Heddergott, D. Dablhaus, and K. T. Perderson, "Channel parameter estimation in mobile radio environments using the SAGE algorithm," *IEEE J. Selected Areas in Comm.*, Vol. 17, 434–450, Mar. 1999.
39. Tan, S. Y. and H. S. Tan, "Improved three-dimensional ray tracing techniques for microcellular propagation models," *IEE Electronics Letters*, Vol. 31, 1503–1505, Aug. 1995.
40. Ang, T. W., S. Y. Tan, and H. S. Tan, "Analytical methods to determine diffraction points on multiple edges and cylindrical scatterers in UTD ray tracing," *Microwave and Optical Technology Letters*, Vol. 22, No. 5, 304–309, Sep. 1999.
41. Sun, Q., S. Y. Tan, and K. C. Teh, "Analytical formulae for path loss prediction in urban street –Grid microcellular environments," *IEEE Trans. Vehicular Technology*, Vol. 54, No. 4, 1251–1258, USA, Jul. 2005.
42. Tan, S. Y., M. Y. Tan, and H. S. Tan, "Multipath delay measurements and modelling for inter-floor wireless communications," *IEEE Trans. Vehicular Technology*, Vol. 49, No. 4, 1334–1341, Jul. 2000.
43. Tan, S. Y. and H. S. Tan, "A microcellular communications propagation model based on uniform theory of diffraction and multiple image theory," *IEEE Trans. Antennas and Propagation*, Vol. 44, No. 10, 1317–1326, Oct. 1996.